Received: 19 October 2023 | Revised: 6 May 2024 | Accepted: 8 May 2024

DOI: 10.1002/mrm.30165

REVIEW

Magnetic Resonance in Medicine

Quantitative BOLD (qBOLD) imaging of oxygen metabolism and blood oxygenation in the human body: A scoping review

Ahlam A. Alzaidi[1,2] | **Rafal Panek**[3] | **Nicholas P. Blockley**[1]

[1]David Greenfield Human Physiology Unit, School of Life Sciences, University of Nottingham, Nottingham, UK

[2]Radiology Department, College of Applied Medical Sciences, Taif University, Taif, Saudi Arabia

[3]Medical Physics and Clinical Engineering, Nottingham University Hospitals NHS Trust, Nottingham, UK

Correspondence
Nicholas P. Blockley, David Greenfield Human Physiology Unit, School of Life Sciences, University of Nottingham, Nottingham, UK.
Email: nicholas.blockley@nottingham.ac.uk

Funding information
Taif University

Abstract

Purpose: There are many approaches to the quantitative BOLD (qBOLD) technique described in the literature, differing in pulse sequences, MRI parameters and data processing. Thus, in this review, we summarized the acquisition methods, approaches used for oxygenation quantification and clinical populations investigated.

Methods: Three databases were systematically searched (Medline, Embase, and Web of Science) for published research that used qBOLD methods for quantification of oxygen metabolism. Data extraction and synthesis were performed by one author and reviewed by a second author.

Results: A total of 93 relevant papers were identified. Acquisition strategies were summarized, and oxygenation parameters were found to have been investigated in many pathologies such as steno-occlusive diseases, stroke, glioma, and multiple sclerosis disease.

Conclusion: A summary of qBOLD approaches for oxygenation measurements and applications could help researchers to identify good practice and provide objective information to inform the development of future consensus recommendations.

KEYWORDS

OEF, oxygen extraction fraction, oxygenation, qBOLD, quantitative BOLD

1 | INTRODUCTION

Baseline oxygen metabolism and blood oxygenation are thought to be affected in a variety of diseases. The gold standard technique for mapping oxygen metabolism is triple oxygen PET, which utilizes ^{15}O-labeled H_2O, O_2, and CO to measure oxygen extraction fraction (OEF), cerebral blood flow (CBF), and cerebral metabolic rate of oxygen consumption ($CMRO_2$).[1,2]PET studies using this technique have shown metabolic changes in ageing,[3] dementia,[4] and Alzheimer's disease.[1] However, the complicated logistics, radiation exposure, and requirement for an onsite cyclotron to create the ^{15}O isotope, which has a short half-life of 2 min, have limited its broad clinical usage.[5,6]

In recent years, advanced MR techniques have been developed to quantify baseline oxygen metabolism. Some of those techniques are based on respiratory calibration of

the BOLD signal,[7,8] whereas other non-respiratory techniques include T_2-based methods,[9,10] susceptibility based methods[11–13] and quantitative BOLD (qBOLD) and R'_2 (reversible transverse relaxation rate) mapping.[14,15,6] Some of these techniques try to estimate oxygen metabolism in specific brain regions, while others provide a global or whole-brain assessment of oxygen metabolism and have been discussed broadly in a recent review[5] by Jiang and Lu, which provides an overview of all MRI-based OEF measurements. However, this review is distinct in two ways. First, the scoping review is a methodology to "systematically map the literature available on a topic, identifying key concepts, theories, sources of evidence and gaps in the research".[16] Second, this review focuses specifically on the quantitative BOLD technique for mapping OEF and R'_2 for assessment of relative tissue oxygenation rather than OEF measurement techniques in general.

1.1 | qBOLD theoretical underpinning

The qBOLD technique establishes a relationship between OEF and the observed MRI signal,[17] and has been shown to be a valid approach for estimating blood oxygenation in preclinical studies[18] and healthy human subjects.[19,20] More recently, it has been used in investigating patients with stroke[21] and glioma.[22]

The qBOLD model focuses on signal decay in the *extravascular* tissue space caused by local magnetic field inhomogeneities surrounding the blood vessel network and induced by paramagnetic deoxyhemoglobin. Traditionally, models of the BOLD signal are unable to separate the contributions of blood oxygenation level (i.e., OEF) and blood volume to the transverse signal decay. Therefore, a faster BOLD signal decay (i.e., a greater value of R'_2) might be caused by either decreased blood oxygenation or increased blood volume. However, Yablonskiy and colleagues developed a model of the BOLD signal in the static dephasing regime (SDR), by modeling the blood vessels as a network of randomly oriented cylinders. This SDR model has the advantage of being able to separate experimentally the oxygenation and blood volume effects. Particularly, two asymptotic equations can be derived to describe the signal behavior in the short and the long-time scales[17,21,23]:

$$S_s = S_0 \cdot e^{-\mathrm{TE}\cdot R_2} \cdot e^{-0.3\cdot(R'_2\cdot\tau)^2/\mathrm{DBV}}, \qquad \tau < \frac{1.5\cdot \mathrm{DBV}}{R'_2} \quad (1)$$

$$S_L = S_0 \cdot e^{-\mathrm{TE}\cdot R_2} \cdot e^{-\tau\cdot R'_2} \cdot e^{\mathrm{DBV}}, \qquad \tau > \frac{1.5\cdot \mathrm{DBV}}{R'_2} \quad (2)$$

where τ is defined as the *spin echo displacement time* which controls the R'_2-weighting of the signal, TE is the echo time, and R_2 is the irreversible transverse relaxation rate. DBV represents the deoxygenated blood volume with the understanding that the veins typically are the major contributor to it. During the short timescale of Eq. (1) the signal decay is quadratically exponential, whereas in the long-time scale in Eq. (2) it is linearly exponential. From this long timescale, it is possible to characterize R'_2 ($R'_2 = R^*_2 - R_2$) as,

$$R'_2 = \mathrm{DBV}\cdot\gamma\cdot\frac{4}{3}\pi\cdot\Delta\chi\cdot\mathrm{Hct}\cdot\mathrm{OEF}\cdot B_0 \quad (3)$$

where γ is the gyromagnetic ratio (2.68×10^8 rad/s/T), B_0 is the main magnetic field strength, Hct is the fractional haematocrit, and $\Delta\chi$ is the susceptibility difference between fully deoxygenated and fully oxygenated blood (0.27 ppm per unit Hct[24]). Therefore, measurements of R'_2 are proportional to deoxyhemoglobin content, that is, the product of hematocrit and OEF. DBV can be calculated via comparison of the measured signal at the short timescale $S_{s(\mathrm{meas})}$ with the intercept extrapolated from long timescale data $S_{L(\mathrm{extrap})}$ using Eq. 4.

$$\mathrm{DBV} = \ln S_{L(\mathrm{extrap})}(0) - \ln S_{S(\mathrm{meas})}(0). \quad (4)$$

Therefore, when R'_2 and DBV are known, OEF can be estimated from Eq. 3.

To assess OEF using the qBOLD model, many studies have used a gradient echo sampling of spin echo (GESSE) sequence, in which multiple gradient echoes are obtained with varying values of τ.[23] However, one disadvantage of this sequence is that the R_2-weighting of the gradient echo signals also varies with τ and must be taken into account when estimating R'_2.[14,15,25] The asymmetric spin echo (ASE) sequence in which the refocusing pulse of a spin echo pulse (SE) sequence is shifted by $\tau/2$ to produce various degrees of R'_2-weighting while keeping the TE constant has also been used. This enables R'_2 to be estimated directly without the confounding effects of R_2-weighting. Both the GESSE and ASE methods require roughly 5–10 min to map the OEF.[26] Since the qBOLD model relies on small differences in the signal decay to distinguish the DBV and OEF effects (Eqs. 1 and 2), a high SNR is required to estimate them from GESSE or ASE data.[19,23,27] To overcome this issue, the multiparametric-qBOLD (mp-qBOLD) approach was devised, in which CBV is evaluated using dynamic susceptibility contrast (DSC) MRI and R'_2 is estimated by separately mapping R_2 with a multiple spin-echo sequence and R^*_2 with a multi-echo GRE sequence.[28,29] Nonetheless the CBV measured by DSC is the total CBV, not the DBV required for qBOLD. As a result, the OEF produced by mp-qBOLD is a relative measure of OEF.[29,30]

The qBOLD model described in Eqs. (1) and (2) considers a single extravascular tissue compartment and assumes that R_2' is only associated with deoxygenated blood. However, R_2' is susceptible to macroscopic magnetic field inhomogeneity, which must be addressed either prospectively with techniques like z-shimming[31] or the use of exponential excitation pulses,[32] retrospectively with a high-resolution field map or by modeling the voxel spread function.[15,33,34] If not, then R_2' will be increased leading to an overestimation of OEF.

Other compartments, such as intravascular blood and CSF or interstitial fluid (ISF), can be found in an in vivo imaging voxel, in the latter case resulting in an increase in R_2'. He and Yablonskiy explain the CSF effect as being caused by its differing protein and lipid content with respect to tissue, resulting in frequency shifts and phase differences in its MR signal relative to the tissue component.[15] To address this, the qBOLD model was expanded to include contributions from GM, WM, CSF, and blood.[15] However, implementing this multi-compartmental model demands prior tissue composition knowledge and involves a large number of fitting parameters.[15] Otherwise, to simplify the model, it is possible to reduce the contributions from other compartments. For instance, it has been proposed that the intravascular contribution can be minimized by employing flow crushing gradients,[26] and the CSF/ISF signal suppressed utilizing a fluid attenuated inversion recovery (FLAIR) preparation pulse.[21] Another key assumption of the qBOLD model is SDR for MRI signal formation in the presence of the blood vessels network which assumes the diffusion effect is negligible. However, it has been demonstrated that diffusion has a vessel size-dependent effect on signal decay, and that disregarding this effect may result in systematic underestimation of OEF.[35–37]

1.2 | Aims of the review

To the best of our knowledge, there is no systematic review detailing the breadth of qBOLD acquisition, processing methods and clinical applications that have been presented and used in the literature. Therefore, the aim of this study is to perform a systematic scoping review of papers which employ the qBOLD technique. We present an overview of the different aspects of the qBOLD experiments reported and applied in the literature, describing the methods and clinical research applications. We classified and analyzed the acquisition, data processing and populations employed and based on these findings we identified recent practices, trends, technical findings, and evidence from clinical studies.

2 | METHODS

The evidence on the applications of the qBOLD approach in the literature was mapped in this systematic scoping review. The scoping review approach[16] provides a summary of existing evidence on a topic in order to reveal the depth and breadth of that topic. These findings are reported based on the Preferred Reporting Items for Systematic Review and Meta-Analysis Extension for Scoping Review (PRISMA-ScR), which also guided the protocol for this scoping review.[38]

2.1 | Search strategy

A systematic search was performed in the following databases: Medline, Embase, and Web of Science. The search strategy combined terms relating to "quantitative BOLD," "qBOLD," "oxygen extraction," "oxygen extraction fraction," "oxygen saturation," "oxygen metabolism," "magnetic resonance," "MRI," "MR imaging," "MR measurements," and "Quantitative measurements of cerebral blood oxygen." The search was constrained to English-language literature and date of publication from 1994, the year in which the theory underlying qBOLD was first reported.[17] Full details of the search strategy are provided in the Appendix. The last updated search was conducted in August 2023.

2.2 | Eligibility criteria

The following inclusion criteria were applied: studies that have been conducted on humans including healthy volunteers or patients. Studies that reported measurement outcomes of oxygenation using qBOLD such as deoxyhemoglobin concentration, deoxyhemoglobin content, OEF, oxygenation, oxygen saturation, R_2'. Studies which only report T_2'/R_2' were also included. T_2' is the reversible transverse relaxation time which is the inverse of R_2' that is, $T_2' = 1/R_2'$. A decrease in T_2' indicates an elevation in deoxyhemoglobin which is equivalent to an increase in R_2'. As shown by Eq. (3), R_2' is proportional to the product of OEF and CBV.

The following exclusion criteria were used: calibrated BOLD or dual calibrated FMRI or QUO_2 using hypercapnia and/or hyperoxia, T_2 Relaxation Under Spin Tagging (TRUST), Susceptibility Based Oximetry (SBO), VAscular Space Occupancy (VASO), Velocity-selective Excitation with Arterial Nulling (VSEAN), Quantitative Imaging of eXtraction of Oxygen and TIssue Consumption (QUIXOTIC), reviews, simulation studies, and preclinical studies.

2.3 | Selection of sources of evidence

The search records from the three databases were transferred to the Endnote (Clarivate, Philadelphia, PA) reference tool, where duplicates were identified and removed. Records were then screened by title and abstract by two researchers (A. A., N. B.). The included studies were transferred to the Rayyan software tool (Rayyan Systems, Inc., Cambridge, MA) and screened independently by title and abstract according to the inclusion and exclusion criteria by two researchers (A. A., N. B.). Disagreements were resolved by consensus. Two researchers (A. A., N. B.) went through the full text of the included papers in a second step checking for their eligibility for final inclusion.

2.4 | Data charting

Data were extracted from each of the selected articles and tabulated. The following characteristics were extracted: study characteristics, such as: author, year, methods, and aim/objective of the study; population characteristics, including sample size, age, pathology. MRI acquisition parameters were recorded including magnetic field strength and type of pulse sequence. The technique for measuring CBV and OEF were documented. Finally, information on the analysis was extracted. Data extraction of all included studies was performed by the lead author (A. A.), and a sample of these data were checked by the senior author (N. B.).

3 | RESULTS

3.1 | Study selection and population characteristics

The electronic search of the three databases retrieved 5172 studies of which 2469 studies remained after checking for duplicates. After screening of abstracts and full texts for eligibility, 119 studies remained for full-text assessment according to the inclusion and exclusion criteria. Finally, 93 studies met the inclusion criteria and were included in the scoping review. Figure 1 presents a Prisma Flow Diagram illustrating the search results.[39] The studies included a total of 3239 participants, comprised of 1809 patients and 1432 healthy participants. Twelve papers did not provide any age information, a further 34 papers reported only the age range. The mean participant age, computed as the group mean weighted by the number of participants in each study, was 43.3 years for healthy participants, while for patients it was 53.1 years.

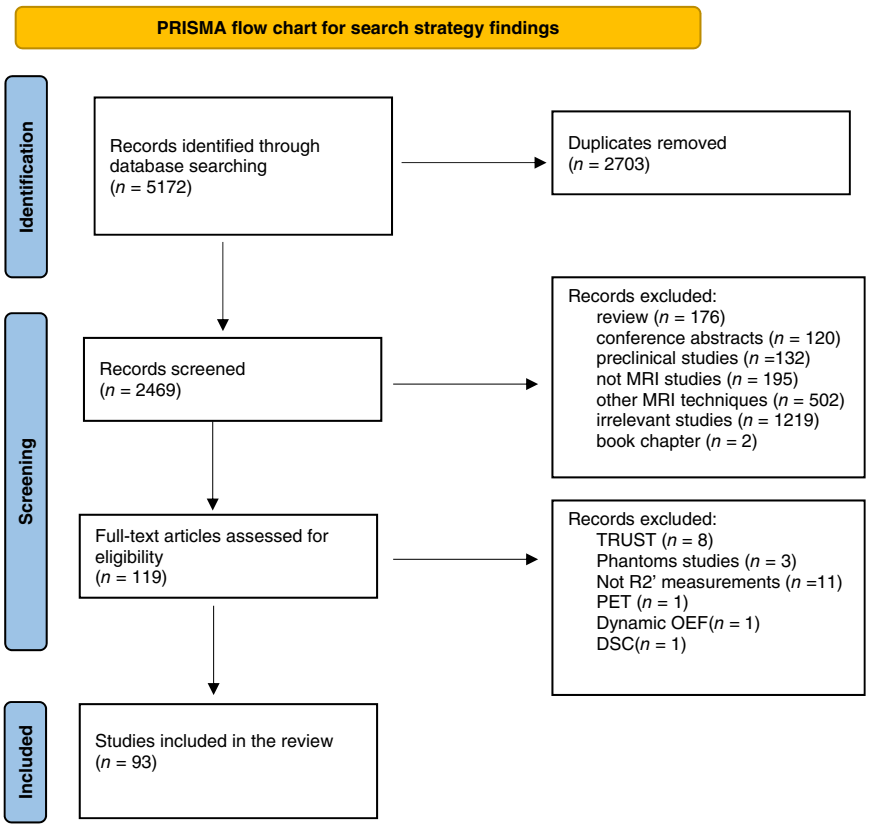

FIGURE 1 PRISMA flow chart for search strategy findings.

3.2 | Acquisition and analysis

The number of included studies that were conducted at 3T is 78/93, where the remainder were acquired at 1.5T (15/93). In this review, we identified many studies of qBOLD with different names such as qBOLD, multi-parametric qBOLD (mqBOLD), quantitative susceptibility mapping combined with qBOLD (QQ), interleaved (iqBOLD) and streamlined qBOLD (sqBOLD). Despite the fact these techniques have different names, some of them are based on the same or similar acquisition methods. Thus, categorizing the included studies based on acquisitions methods revealed four main acquisition methods. Multiparametric acquisitions (mp-qBOLD) consisting of separate acquisitions of R_2^* and R_2, which is the most common approach in the literature (36 studies) and has been applied in a slightly diverse way regarding the pulse sequence applied and the approach for measuring CBV, followed by ASE (21) which has been applied mainly using the basic ASE pulse sequence, and other branches of the ASE pulse sequences , such as MASE used in one study and GASE in two studies, gradient-echo (GRE) (19), GESSE (12), spin and gradient echo (SAGE) (2), and gradient-echo sampling of free induction decay and echo (GESFIDE) (2) (see Table 1 for a full reference list and Figure 2). Median and range of MRI parameters of the most common qBOLD acquisitions are presented in Table 2. On the clinical side, the most commonly used acquisition is the multiparametric approach, specifically mp-qBOLD (GRE and SE), followed by ASE, GRE, GESSE, and mp-qBOLD (GRE and gradient and spin-echo [GRASE]), then mp-qBOLD (SE and EPI), and finally SAGE.

Table 3 presents the mean of R_2', DBV and OEF values for healthy volunteers across studies characterized

TABLE 1 Pulse sequences applied in mp-qBOLD acquisition and the way of measuring CBV or DBV.

Pulse sequence	No. of studies References	CBV/DBV via
mp-qBOLD		
Multi gradient echo/multi spin echo	15[22,25,28,6,40–50]	DSC[22,25,28,6,40–50]
Multi gradient echo/fast-spin echo	4[51–54]	DSC[53]
Multi-gradient echo/gradient and spin echo (GRASE)	7[29,30,55–59]	DSC[29,30,55–59]
Gradient echo-EPI/fast-spin echo	6[60–65]	DSC[61]
Multi gradient echo/fast-multi spin echo	2[66,67]	-
Fast-gradient echo/fast-spin echo	2[68,69]	-
ASE		
ASE	11[21,70–80]	Yablonskiy and Haacke qBOLD model[17]
Triple-echo ASE	4[81–84]	Yablonskiy and Haacke qBOLD model[17]
Multi-echo-ASE	1[85]	Yablonskiy and Haacke qBOLD model[17]
ASE-velocity-selective spin-labelling (VSSL)	1[86]	Yablonskiy and Haacke qBOLD model[17] aided with VSSL maps
ASE-VASO	1[87]	Yablonskiy and Haacke qBOLD model[17]
Electrocardiogram-triggered ASE	1[88]	Yablonskiy and Haacke qBOLD model[17]
GESSE		
Gradient echo sampling of spin echo (GESSE)	12[14,15,19,37,89–94]	Yablonskiy and Haacke qBOLD model[17]
Multi-gradient echo		
Multi-gradient echo	19[19,34,95–112]	QQ model[85,95,97–106,108,111] Yablonskiy and Haacke qBOLD model[17,34,96,109,110]
GESFIDE		
Gradient echo sampling of fid and echo (GESFIDE)	2[113]	Yablonskiy and Haacke qBOLD model[17]
SAGE		
SAGE	2[114,115]	Yablonskiy and Haacke qBOLD model[17]

Abbreviations: ASE, asymmetric spin echo; CBV, cerebral blood volume; DBV, deoxygenated blood volume; DSC, dynamic susceptibility contrast.

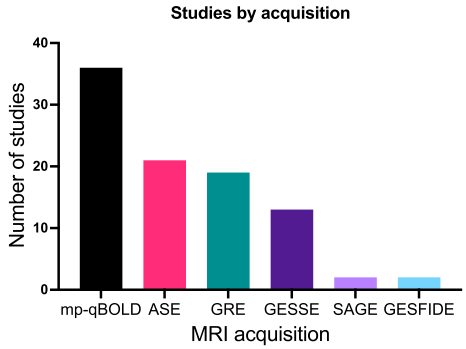

FIGURE 2 Acquisitions used for acquiring qBOLD data by number of studies. mp-qBOLD, multiparametric qBOLD; ASE, asymmetric spin echo; GRE, gradient echo; GESSE, gradient echo sampling of spin echo; SAGE, spin and gradient echo; GESEFIDI, a gradient-echo sampling of free induction decay and echo.

by acquisition type. The mp-qBOLD acquisition seems to provide higher values overall compared to ASE and GESSE. Accounting for magnetic field inhomogeneity (MFI) was performed in 41% of the included studies with different approaches, including prospective correction using exponential excitation pulses (12%)[31,6,40,55,56,66,68,128] or z-shimming (5%),[21,41,70,71,120] model fitting (1%),[89] slice averaging (1%),[28] voxel spread function (4%),[34,95–97] projection onto dipole field (12%),[95,98–108] and retrospective correction using field maps (8%).[15,25,37,86,90,109] In addition, ~6% of the studies used FLAIR to suppress the CSF/ISF signal.[21,67,70,71,86,120]

Common pre-processing steps that were reported were motion correction, spatial smoothing and registration to MNI or subject space. However, 21 studies did not report pre-processing steps.[14,25,42,60–63,68,81–83,89–92,99–101,113,116–117] The method of the analysis was mostly region of interests (ROIs), including WM, GM, and whole brain analysis (63 studies) or ROIs combined with voxel-wise analysis (5 studies).[56,66,72,73,124] OEF maps were mostly computed by using least squares fitting (18 studies),[14,15,21,25,30,34,37,57,71,74–76,84–85,88,90,96,109,114] but in one study, Bayesian inference was used.[70] Further advanced analysis approaches such as cluster analysis of time evolution (CAT) and artificial neural network (ANN) have been applied in nine studies.[89,98,101,102,105,107–108,110–111] The main principle behind the CAT method is that voxels with a similar mGRE signal evolution have similar model parameter values, and the number of clusters as defined by machine learning is less than the number of voxels. Hence, averaging over a cluster can substantially improve SNR for a cluster-wise inverse solution that can be utilized as a robust initial estimate for voxel-wise QSM + qBOLD

TABLE 2 Median and range (in square brackets) for MRI parameters used in qBOLD or R_2' mapping studies.

Technique Parameters	ASE	GESSE	mp-qBOLD(SE)	mp-qBOLD(GRE)
No. of echoes	N/A	26 [10–89]	8 [4–32]	8 [8–28]
TR (ms)	5000 [3000–5000]	5000 [3000–5000]	2600 [1000–10 000]	1210 [67–75 000]
TE (ms)	62 [62–82]	62 [62–82]	16 [8.8–17]	5 [5–10]
Delta TE (ms)	N/A	4 [2–4.96]	15 [6.43–42.75]	6 [5–7]
Time of SE (ms)	N/A	64 [32.8–133.29]	N/A	N/A
τ (ms)	10[−16–22.5]	-	N/A	N/A
Δ τ (ms)	0.5 [0.5–8]	-	N/A	N/A
Spatial resolution (mm)	3 × 3 [2.29–3 × 2.29–3]	3 × 3 [2.29–3 × 2.29–3]	1.8 × 1.8 [0.86–2.5 × 1–2.5]	1.25 × 1.3 [0.86–2.5 × 1–2.5]
FOV (mm)	192 × 192 [192–220×-192–220]	248 × 256 [160–256 × 192–256]	240 × 203[208–320 × 156–256]	240 × 182 [200–240 × 160-240]
No. of slices	16 [9–19]	1 [1–9]	25 [4–50]	27 [8–75]
Slice thickness (mm)	3 [3–5]	7.5 [3–8]	4 [2–6]	2[0.8–6]
Acquisition time (mins:sec)	5:48 [3:48–9:36]	12.54 [8:30–21:07]	3.5 [2.5–12.14]	3:36 [1:05–8:00]
No of studies	7	10	24	24
References	71, 73, 75–79	14, 15, 25, 37, 89–90, 94, 105, 116	22, 28, 6, 40–53, 65–66, 68–69, 117–119	10, 42, 48, 60–62, 81–82, 86, 89, 91–92, 98–101, 113, 116–117, 120–123

Note: Only studies with mostly complete descriptions of the relevant parameters were included.

TABLE 3 Mean and range of R'_2, DBV and OEF values in brain tissue for healthy volunteers across studies categorized by acquisition type.

qBOLD acquisition	R'_2 (Hz)	DBV (%)	OEF (%)
GESSE	4.69 [2.90–6.70][15,25,37,90]	4.56 [1.75–4.59][14,15,25,37,44,89–90,105]	37.16 [31.60–46.30][14,15,19,25,37,89–93,105]
ASE	3.10 [2.60–3.60][21,70]	5.9 [3.10–6.70][21,70,85,86]	32.66 [21.0–40.0][21,70,74,76,85,86,124–125]
mp-qBOLD	6.76 [4.43–8.10][28,29,60,63,68,90,126–127]	6.21 [4.30–9.20][28,90]	52.0 [29.10–60.0][28,29,55–57,90]
GRE (QQ)[a]	N/A	2.8 [1–4.5][95,101,102,104]	36.4 [30.6–43.8][95,101,102,104]

Abbreviations: ASE, asymmetric spin echo; DBV, deoxygenated blood volume; GESSE, gradient echo sampling of spin echo; GRE, gradient-echo; OEF, oxygen extraction fraction.

Note: Means are weighted by the number of participants in each study.

[a]Only values from the QQ approach are included for the GRE acquisition.

optimization.[102] Alternatively, ANN is a machine learning tool used to recognize patterns and classify data. It has proven to be an effective alternative approach for robust curve fitting, with good noise and outlier resilience and faster computational processing compared to least squares fitting.[89] Some of the studies did not provide detailed information about the fitting procedure that was used.[43,81–83,92–93,116,124] The most common software tools used for analysis are MATLAB (Mathworks, Natick, MA), FSL,[129] and SPM.[130]

3.3 | Applications

The most investigated human organ was the brain (84 studies, see supplementary information for full studies details), followed by lower extremity muscle (4 studies),[15,81,83,84] breast (2 studies),[6,42] liver (1 study),[109] spinal cord (1 study),[115] and heart (1 study).[57] The majority of brain studies used the mp-qBOLD approach for acquisition (34 studies),[22,25,28–30,6,41–47,51–53,55–58,60–66,68–69,116–118,128] followed by GESSE acquisition (12 studies),[14,15,19,37,89–94] then ASE (11 studies).[19,21,70,71,73–75,77–78,85–86,124] Studies conducted on the breast used the mp-qBOLD approach.[6,42] However, in the lower extremities, all the studies used ASE.[81–84]

Twenty-eight studies explored using qBOLD methods on healthy subjects for various aims, such as to assess the technical feasibility of the qBOLD method,[15,28,37,79,84,88,95] and to develop a new related qBOLD technique.[21,86] Furthermore, validation studies were also performed to investigate the validity of the technique and the model[19,25,99] as well as making MRI versus PET comparisons.[56,103] On the other hand, 64 out of 93 studies (64/93) investigated diseases to measure tissue hemodynamic parameters, such as blood volume, deoxyhemoglobin concentration, and OEF as well as measuring T'_2 or R'_2 as a surrogate marker of local oxygenation. Cerebrovascular diseases, for example, stroke, carotid stenosis/occlusion, mitochondrial myopathy, encephalopathy, lactic acidosis, and stroke-like episodes (MELAS), were the most investigated diseases (28 studies), followed by glioma and brain tumor (17), diabetes (3),[19,81,82] hemoglobinopathies (4),[19,72,73] breast tumor (2),[6,42] multiple sclerosis (MS) (2),[63,100] clinically isolated syndrome (CIS) (2),[19,60] pre-eclampsia (PE) (2),[106,108] neurodegenerative disease (2),[19,107] human immunodeficiency virus (HIV) (2),[76,80] and 1 study for the following diseases: cervical spondylosis,[115] retinal vasculopathy with cerebral leukoencephalopathy and systemic manifestations (RVCL-S)[78] (Figure 3). Table 4 lists the most common pathologies investigated along with clinical finding related to oxygenation parameters.

Studies have also been performed outside of the brain. Oxygenation parameters have been measured in lower body extremities, in particular in the calf muscle, using qBOLD in patients with diabetes.[81–83] The measurements were performed at rest and during an isometric plantar flexion muscle contraction, Zheng and colleagues reported

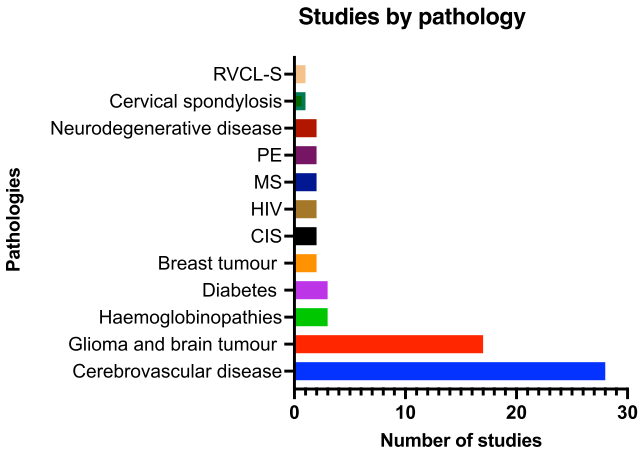

FIGURE 3 Number of studies for each of the pathologies investigated using qBOLD or R'_2 mapping. CSI, clinically isolated syndrome; HIV, human immunodeficiency virus; MS, multiple sclerosis; PE, pre-eclampsia; RVCL-S, cerebral leukoencephalopathy and systemic manifestations.

TABLE 4 Findings of most common pathologies investigated using qBOLD or R_2' mapping.

Pathology	No. of studies	Findings
Cerebrovascular diseases	28	• Low OEF in DWI-defined lesions in ischemic stroke patients.[101,102] • Different OEF histogram compared to the contralateral side in ischemic stroke patients.[102] • Lower OEF in the ipsilateral side compared to the contralateral side in ischemic stroke patients.[98] • Infarct core OEF value showed decreasing trend from acute to early subacute to late subacute phases of ischemic stroke[110] • rCBV and OEF were unchanged, whereas $rCMRO_2$ and CBF had a relative reduction in the affected side with the stenosed carotid artery.[127] • rOEF was unchanged in asymptomatic internal carotid artery stenosis (ICAS) patients[55] • Elevation of rOEF and CBF preoperatively which reduced to normal range following surgery in patients with severe cerebrovascular stenosis or occlusive disease.[91] • Decrease in the T_2' value in the affected side compared to the contralateral in acute stroke patients[64] • Lower T_2' values within hypoperfused tissue in acute ischemic stroke patients.[51,52,64] • Higher T_2' values in hyperperfused area in acute ischemic stroke patients.[52,64] • T_2' values in clinically isolated syndrome (CIS) did not differ significantly from healthy control[62]
Glioma and brain tumor	17	• Higher OEF in ipsilateral side and suspected tumor area.[22,47,53,66,89,90,114,128] • Low-grade glioma showed areas with increased OEF, whereas anaplastic glioma (grade III) and glioblastoma (grade IV) showed decreased OEF when compared with normal brain tissue.[47,128] • OEF distinguishing Isocitrate dehydrogenase IDH1 status and mutant gliomas in the tumor area.[119] • OEF was lower in glioblastomas than metastases.[48,111]
Diabetes	3	• Diabetic patients had lower OEF and oxygen consumption compared to healthy controls.[82,83,131]
Hemoglobinopathies	4	• Sickle cell anemia (SCA) patients showed variation in whole-brain OEF and decreased values of OEF in white matter at higher risk of stroke under different treatment options.[73,132] • Increase OEF within normal appearance white matter of SCA patients compared to healthy control.[124] • Whole brain OEF values was higher in SCA patients compared to healthy control.[72]

Abbreviations: CBF, cerebral blood flow; DWI, diffusion-weighted imaging; OEF, oxygen extraction fraction.

an attenuated oxygenation response during isometric calf muscle exercise in people with diabetes mellitus compared to a non-diabetic group.[81–83] In breast cancer, two studies have been conducted using the mp-qBOLD acquisition approach with DSC to assess the viability of using qBOLD as a non-invasive way to assess the tumor microenvironment (TME), hypoxia, and induced neovascularization. It aimed to differentiate between aggressive and less aggressive breast cancer.[6,42] Findings from these studies suggested that mp-qBOLD can aid in the non-invasive identification of aggressive breast cancer. Two studies[106,108] have been conducted to investigate brain oxygen metabolism in pregnant women with pre-eclampsia, which causes high blood pressure. The studies found that women with pre-eclampsia had higher OEF values than healthy pregnant women.

4 | DISCUSSION

We identified 93 papers which used qBOLD to quantify oxygenation-related parameters which together included 3239 subjects. Multiple approaches to qBOLD acquisition and analysis were included in this review, of which 41% reported performing correction for magnetic field inhomogeneity (prospective or retrospective) and 6% reported

performing correction for the presence of CSF. Studies were conducted in six organs, although 91% studied the brain, and 12 different pathologies, with the vast majority investigating cerebrovascular disease (44%) or glioma and brain tumors (27%).

4.1 | Reporting standards

Most studies reported the acquisition details except seven ASE studies which referred to other papers for more details; this leaves room for ambiguity on how the actual data were acquired. Another three ASE studies reported using triple-echo ASE but did not give enough details on how these data were analyzed. Seven mp-qBOLD papers and two GESSE papers reported incomplete information about MRI acquisition parameters. Oxygenation maps were mainly computed using simple iterative least-squares regression.[90] However, in studies using the QSM + qBOLD technique, machine learning algorithms such as artificial neural networks (ANNs) have been applied with the aim of improving the robustness of curve-fitting.[89,100–102,104] More than half of studies did not report the fitting method details clearly. Reporting more details about both acquisition and processing methods would enable more reliable replication and comparisons of these methods.

4.2 | Acquisition and analysis

The majority of qBOLD studies were performed at 3T using the mp-qBOLD approach (GRE and SE) for data acquisition, followed by the ASE sequence. While qBOLD can be performed using different sequences to measure oxygenation parameters, all have limitations. Because the qBOLD signal is a function of R_2' and DBV, alterations in acquiring these parameters can affect the final outcomes, that is, OEF. For instance, acquiring R_2' with different acquisitions has been shown to produce significantly different values.[133] This is particularly the case for the mp-qBOLD approach due to the multiple techniques in use to measure T_2, each with different sensitivities to RF pulse errors leading to overestimation of T_2 and underestimation of R_2'.[29] However, from the literature reviewed in this review, there was a notable difference in the estimate of R_2' between the GESSE and ASE techniques which both have a direct sensitivity to R_2'. When compared with GESSE measurements of R_2', mp-qBOLD measurements of R_2' are 47% higher, whereas ASE measurements are 34% lower. Simulations have shown that the differences in measurements of R_2' using GESSE and ASE may be due to the effect of diffusion. In the GESSE technique, the amount of time for protons to diffuse around the blood vessels increases with TE which flattens the signal decay around the spin echo.[37] In contrast, this time for proton diffusion is fixed for the ASE technique and equally affects all of the τ values (R_2'-weightings).[35] While for mp-qBOLD, the higher R_2' measurements are believed to be due to stimulated echoes due to slice-selection pulse imperfections, in 2D-GraSE and 2D-TSE imaging that lead to T_2 overestimations, hence, higher R_2' measurements. To overcome these issues, it is advisable to use non-slice selective and 3D acquisition techniques, such as 3D-GraSE, to reduce T_2-related bias in mp-qBOLD.[29] R_2' values for the QQ approach are not available since this model fits directly for OEF and DBV. The R_2' measurements reported from the included studies highlighted the notion that R_2' measurements are clearly influenced by the acquisition method (Table 3), which also has been reported previously.[133] This is an important consideration for designing and evaluating research that use R_2' measurements. In addition, R_2' measurements are influenced by the orientation of the white matter fibers[32] and the existence of myelin, which has a high diamagnetic susceptibility. Each voxel's signal decay becomes multi-exponential due to the presence of extracellular, intracellular, and myelin water compartments. Previous studies have shown that a significant frequency shift is caused by the water compartmentalization in the myelin, which increases the R_2^* decay during gradient echoes.[134,135]

It is crucial to distinguish between the susceptibility effects caused by deoxyhemoglobin and those caused by static field inhomogeneities to get a more accurate estimation of R_2'. To recover signal loss or separate the impacts of these two field fluctuations, a number of techniques have been applied in the included studies. The most common ways were as follows, applying an exponential excitation pulse,[30,6,40,55,56,66,68,128] using high-resolution field maps,[15,25,37,86,90,109] z-shimming,[21,41,70,71,120] and voxel spread function.[34,95–97] However, these techniques have inherent limitations, and the choice of approach relies on the particular application and the resources at hand. Furthermore, accounting for the presence of partial volumes of CSF is important. However, few studies considered suppressing CSF/ISF signal by using a FLAIR preparation pulse.[21,67,70,71,86,120]

The DBV is similarly measured in different ways (Table 3). In the qBOLD model, the DBV is estimated from the transverse signal decay, but this method has potential issues, including signals from intravascular blood,[26] diffusion narrowing effects,[35] and signals from macromolecules.[15] On the other hand, in mp-qBOLD, the DBV measure is replaced by the DSC measure of cerebral blood volume (CBV). This CBV measure is combined with a separate measurement of R_2' to estimate OEF. However, it is important to note that DBV in the qBOLD model specifically refers to the percentage of CBV that contains

deoxyhemoglobin. This leads to a discrepancy between DBV, which is specific to vessels carrying deoxygenated blood, including veins, and CBV from DSC, which is sensitive to all vessel types and represents total blood volume. Although estimating CBV separately results in a relative measure of OEF,[30] it is perhaps a more pragmatic approach for clinical settings. However, when compared with GESSE measurements of DBV, mp-qBOLD measurements of DBV are 48% higher, ASE measurements are 9% higher and GRE measurements using QQ analysis are 39% lower (Table 3). It is worth noting that the QQ approach derives its sensitivity to DBV from the same source as GESSE and ASE measurements (Eq. 4). One of the included studies introduces a new approach which relies on velocity selective spin labelling (VSSL) pulses to measure DBV non-invasively.[86] For comparison, the only other technique for measuring DBV, which uses the BOLD response to a hyperoxia challenge, estimates DBV to be between 2.2 and 8.2%.[121,136]

Regarding the QQ approach, by integrating both qBOLD and QSM there is the potential to counterbalance each of their limitations. One of the drawbacks of the qBOLD model, which neglects non-blood sources of magnetic susceptibility (e.g., myelin), is addressed by QSM, which is able to measure the total magnetic susceptibility regardless of its origin. Conversely, QSM does not directly factor in DBV and assumes a linear relationship with CBF. In this symbiotic relationship, both approaches complement each other, potentially resulting in a more comprehensive methodology where the strengths of one method offset the weaknesses of the other.[5,103] This method has recently been validated against PET. Findings showed, the average OEF values across subjects did not significantly differ between QSM + qBOLD and[16] O-PET,[103] but there was no report of correlation between the two methods.

The considerably higher proportion of studies (40%) using the mp-qBOLD approach is likely due to its reliance on pulse sequences that are already available on the scanner (i.e., SE or GRE). This makes it easier to implement in a clinical setting whereas techniques like ASE and GESSE require custom pulse sequences. This is also true for the QQ approach which utilizes a standard multiecho GRE pulse sequence, so long as magnitude and phase data can be reconstructed on the scanner. mp-qBOLD approaches are also the most common in the brain and ASE is the only technique used in the lower extremities. This is likely due to slow changes in OEF in the clinical brain applications listed in the results, which are suited to the multishot approaches used in mp-qBOLD acquisitions. ASE is a much more rapid acquisition, aiding the measurements of the transient changes in muscle during hyperemia. It is important to note that for fMRI studies of changes in brain oxygen metabolism the calibrated BOLD technique is more suited due to its higher temporal resolution. Studies using qBOLD on other parts of the human body were limited. Nonetheless, existing studies outside of the brain and muscle demonstrate the potential for investigating diseases elsewhere in the human body using qBOLD.

Although qBOLD provides a non-invasive approach for assessing OEF, in the context of a clinical setting, it might be impractical to apply. However, mp-qBOLD provides great applicability in clinical settings due to the MRI protocol availability.

4.3 | Applications

qBOLD was used to measure baseline oxygenation parameters in several pathologies including steno-occlusive diseases, stroke, and small vessel disease (Figure 3 and Table 4). Findings from these investigations showed that ischemic stroke patients had lower OEF in the core infarcted region (tissue that is unsalvageable) than the contralateral region of the brain and a decreasing trend from acute to early subacute to late subacute phases of ischemic stroke. However, there was an OEF elevation in the penumbral region (tissue that may be salvageable with treatment), which typically surrounds the core infarct, compared with healthy tissue in the contralateral hemisphere was also reported.[98,101,110] The penumbra region suffers from a lack of blood flow and can recover if the blood supply can be restored in a timely manner.[137] In terms of T_2', it has been observed to be reduced in the infarct core, as defined by a thresholded ADC map, when compared with healthy tissue.[51,64] Similar but smaller reductions are seen within hypoperfused tissue regions of interest defined by time-to-peak (TTP) by DSC.[52] These decrease in T_2', or equivalently increases in R_2', suggest a more rapid signal decay due to the higher than normal deoxyhemoglobin content of the tissue, which is a consequence of elevated OEF caused by hypoperfusion and/or increase in DBV.[51,64] These findings are consistent with our current understanding of the pathophysiology from PET imaging. According to PET studies, there should be a significant rise in OEF in the penumbra.[125] However, within the core infarct, there is the potential for disagreement with PET. In PET imaging, oxygen metabolism is observed to be reduced within the core,[138] while T_2' has been observed to decrease consistent with an increase in oxygen metabolism.[53] However, Geisler et al. were able to reconcile this discrepancy in the following way.[64] PET relies on an intravascular tracer which cannot reach the core due to a compromised blood supply yielding a negligible oxygen metabolism,[51] whereas measurements of R_2' do not rely on the delivery of a tracer and, hence, are directly

sensitive to the deoxyhemoglobin which remains in the core due to highly reduced blood flow.

Obtaining qBOLD-based OEF measurements for ischemic stroke is particularly challenging due to two main reasons. First, it requires a long acquisition time to obtain high spatial resolution images or many TEs, which can lead to patients moving during the process. This is a common issue with stroke patients that requires motion correction, resulting in additional data acquisition[52,71,116] or image artifacts.[71] Second, using the same Hct value for ischemic and non-ischemic regions can lead to an overestimation of OEF.[71,116] It is also important to note that certain factors such as necrosis, bleeding, iron deposition, fiber orientation, CSF, or macroscopic magnetic susceptibility gradients may cause artificially high OEF values field.[21,64,65,71]

Studies conducted in patients with glioma and brain tumors reported consistent results of higher OEF in the ipsilateral side and suspected tumor area.[53,89,90] Moreover, high-grade glioma revealed higher OEF values than lower-grade glioma.[22,47,66,114,128] However, the heterogeneous nature of gliomas, with different cellular densities, and blood flow patterns, represent a source of bias when merging all types of gliomas into the same group-grade.[61,114] Moreover, it is possible that the necrotic tissue in tumors is susceptible to hemorrhage in the necrotic core, which may result in high R_2' values.[66] Even if there is no bleeding, necrotic tissue can still be problematic because its relative CBV (rCBV) is zero. Therefore, OEF may increase above any physiologically significant threshold.[66] In patients with MS, the reported finding indicated higher OEF values in the rim area compared to the lesion and lower OEF for the whole brain in MS patients compared to healthy control patients.[100] Two studies attempt to evaluate hypoxia in breast cancer, which is a prevalent feature of malignant tumors and is associated with poor treatment outcomes using qBOLD.[6,42] They calculated various quantitative MRI biomarker maps, such as OEF and metabolic rate of oxygen (MRO_2), using histopathology as a standard of reference. The findings demonstrated that invasive ductal carcinomas (IDCs) were more hypoxic than benign tumors.[6] Also, aggressive malignancies had a greater oxygen consumption than less aggressive cancers.[42] It seems qBOLD is a promising technique for measuring baseline oxygenation parameters in a broad range of pathologies and promising direction for some clinical populations.

4.4 | Implications for future research

The application of qBOLD experiments can vary substantially, particularly in the sequence chosen that is ASE, GESSE, and mp-qBOLD. This induces heterogeneity in the outcome measurements of R_2' making it difficult to compare the results of different studies. As yet, there does not seem to have been a direct comparison of a variety of these techniques to assess any systematic differences. However, it should be noted that this is difficult to achieve in human participants due to the normal variation in OEF which can be caused by natural variations in blood carbon dioxide levels.[139] Therefore, phantom based comparisons may be needed. Among the included studies, phantoms were used for several purposes including testing post-processing techniques for correcting for macroscopic magnetic field inhomogeneity.[30,37] One study used gadolinium-doped agar gel phantoms to produce a range of T_2 values to test the accuracy of an improved T_2 measurements as part of an mp-qBOLD approach.[29] However, these kinds of phantoms are not useful for comparing techniques for measuring R_2' because they have little to no R_2' contrast. One further study sought to introduce R_2' contrast by randomly coiling polypropylene strings in mineral oil to generate the mesoscopic magnetic field inhomogeneity that underlies the qBOLD signal.[19] This scoping review was not targeted at phantom comparisons and so the literature captured may be incomplete. However, these studies provide a future direction for phantoms to compare qBOLD variants or between scanners, which might be particularly important for multicentre studies. In addition, validation with the gold standard PET imaging is important; however, this is challenging due to the invasive nature involved in applying PET when using the radioactive agents and its limited availability.

In addition, as noted above, there are multiple techniques in use for estimating DBV, which are not directly comparable. Thus, caution must be taken when reporting OEF results, which are greatly reliant on the pulse sequence and the way in which DBV is estimated. This is true in the case of mp-qBOLD, which does dose not exactly reflect the deoxygenated blood which qBOLD measures. However, since the mp-qBOLD approach is more applicable in clinical settings, it would be worth investigating a more precise way to measure the DBV; one alternative option to DSC-based measurements of CBV is to use hyperoxia-BOLD contrast to measure venous CBV (CBVv).[121] Preliminary work has been presented to demonstrate this approach.[122]

When using qBOLD to measure OEF in conditions such as stroke and glioma, it is important to consider several factors that can impact the accuracy of OEF and R_2' measurements. These factors may include bleeding and necrosis. Using multiple MRI sequences, such as diffusion-weighted imaging (DWI) and perfusion-weighted imaging (PWI), can help provide additional information and enable differentiation

between various tissue compartments, including areas that may be affected by bleeding or necrosis. In addition, correlating findings from different qBOLD approaches with histopathological analysis of tissue specimens can validate the accuracy of OEF measurements and help interpret discrepancies arising from factors like necrosis, hemorrhage, or cellular infiltration.

Public availability of analysis tools is currently limited, with only a single example identified, that is, Quantiphyse.[70,123] However, this tool is only optimized for the ASE acquisition. In future, greater availability of these tools would help to promote reproducibility and harmonization.

4.5 | Limitations of the review

This review was limited to human studies. Therefore, it does not present detail regarding preclinical qBOLD methodologies. However, the basic processing techniques are similar. In addition, it only included studies in the English language due to the long process of translation and time limitations. To date, there has not been a systematic review of the use of qBOLD techniques for measuring blood oxygenation in the human body. Therefore, this review is the first to cover this topic and highlight the use of qBOLD in clinical populations.

5 | CONCLUSIONS

While qBOLD for measuring oxygen metabolism is a relatively underdeveloped technique, we identified applications in several clinical populations including cerebrovascular diseases, brain tumor and glioma, multiple sclerosis, breast cancer, and diabetes mellitus. This highlights the value of qBOLD oxygenation measurements in clinical research. However, acquisition techniques and analysis methods all varied substantially. Future work ought to aim toward consensus recommendations to facilitate more reliable and harmonized qBOLD measurements for use in clinical research and trials of new therapies.

ACKNOWLEDGMENTS

The authors thank Taif University for funding a PhD studentship for AA.

ORCID

Ahlam A. Alzaidi https://orcid.org/0009-0004-8807-4895

Nicholas P. Blockley https://orcid.org/0000-0003-2595-8285

REFERENCES

1. Ishii K, Kitagaki H, Kono M, Mori E. Decreased medial temporal oxygen metabolism in Alzheimer's disease shown by PET. *J. Nucl. Med*. 1996;37:1159-1165.
2. Ito H, Kanno I, Kato C, et al. Database of normal human cerebral blood flow, cerebral blood volume, cerebral oxygen extraction fraction and cerebral metabolic rate of oxygen measured by positron emission tomography with 15O-labelled carbon dioxide or water, carbon monoxide and oxygen: a multicentre study in Japan. *Eur J Nucl Med Mol Imaging*. 2004;31:635-643.
3. Yamaguchi T, Kanno I, Uemura K, et al. Reduction in regional cerebral metabolic rate of oxygen during human aging. *Stroke*. 1986;17:1220-1228.
4. Nagata K, Maruya H, Yuya H, et al. Can PET data differentiate Alzheimer's disease from vascular dementia? *Ann N Y Acad Sci*. 2000;903:252-261.
5. Jiang D, Lu H. Cerebral oxygen extraction fraction MRI: techniques and applications. *Magn Reson Med*. 2022;88:575-600.
6. Stadlbauer A, Zimmermann M, Bennani-Baiti B, et al. Development of a non-invasive assessment of hypoxia and neovascularization with magnetic resonance imaging in benign and malignant breast tumors: initial results. *Mol Imaging Biol*. 2019;21:758-770.
7. Gauthier CJ, Hoge RD. Magnetic resonance imaging of resting OEF and CMRO2 using a generalized calibration model for hypercapnia and hyperoxia. *Neuroimage*. 2012;60:1212-1225.
8. Bulte DP, Kelly M, Germuska M, et al. Quantitative measurement of cerebral physiology using respiratory-calibrated MRI. *Neuroimage*. 2012;60:582-591.
9. Thulborn KR, Waterton JC, Matthews PM, Radda GK. Oxygenation dependence of the transverse relaxation time of water protons in whole blood at high field. *Biochim Biophys Acta*. 1982;714:265-270.
10. Li W, van Zijl PC. Quantitative theory for the transverse relaxation time of blood water. *NMR Biomed*. 2020;33:e4207.
11. Weisskoff RM, Kiihne S. MRI susceptometry: image-based measurement of absolute susceptibility of MR contrast agents and human blood. *Magn Reson Med*. 1992;24:375-383.
12. Haacke E, Tang J, Neelavalli J, Cheng Y. Susceptibility mapping as a means to visualize veins and quantify oxygen saturation. *J Magn Reson Imaging*. 2010;32:663-676.
13. Zhang J, Liu T, Gupta A, Spincemaille P, Nguyen TD, Wang Y. Quantitative mapping of cerebral metabolic rate of oxygen (CMRO2) using quantitative susceptibility mapping (QSM). *Magn Reson Med*. 2015;74:945-952.
14. An HY, Lin WL. Quantitative measurements of cerebral blood oxygen saturation using magnetic resonance imaging. *J Cereb Blood Flow Metab*. 2000;20:1225-1236.
15. He X, Yablonskiy DA. Quantitative BOLD: mapping of human cerebral deoxygenated blood volume and oxygen extraction fraction: default state. *Magn Reson Med*. 2007;57:115-126.
16. Arksey H, O'Malley L. Scoping studies: towards a methodological framework. *Int J Soc Res Methodol*. 2005;8:19-32.
17. Yablonskiy DA, Haacke EM. Theory of NMR signal behavior in magnetically inhomogeneous tissues: the static dephasing regime. *Magn Reson Med*. 1994;32:749-763.
18. He X, Zhu M, Yablonskiy DA. Validation of oxygen extraction fraction measurement by qBOLD technique. *Magn Reson Med*. 2008;60:882-888.

19. Sedlacik J, Reichenbach JR. Validation of quantitative estimation of tissue oxygen extraction fraction and deoxygenated blood volume fraction in phantom and in vivo experiments by using MRI. *Magn Reson Med*. 2010;63:910-921.
20. Yablonskiy DA, Sukstanskii AL, He X. Blood oxygenation level-dependent (BOLD)-based techniques for the quantification of brain hemodynamic and metabolic properties – theoretical models and experimental approaches. *NMR Biomed*. 2013;26:963-986.
21. Stone AJ, Blockley NP. A streamlined acquisition for mapping baseline brain oxygenation using quantitative BOLD. *Neuroimage*. 2017;147:79-88.
22. Wiestler B, Kluge A, Lukas M, et al. Multiparametric MRI-based differentiation of WHO grade II/III glioma and WHO grade IV glioblastoma. *Sci Rep*. 2016;6:6.
23. Yablonskiy DA. Quantitation of intrinsic magnetic susceptibility-related effects in a tissue matrix. Phantom study. *Magn Reson Med*. 1998;39:417-428.
24. Spees WM, Yablonskiy DA, Oswood MC, Ackerman JJ. Water proton MR properties of human blood at 1.5 tesla: magnetic susceptibility, T1, T2, T, and non-Lorentzian signal behavior. *Magn Reson Med*. 2001;45:533-542.
25. An H, Lin W. Cerebral oxygen extraction fraction and cerebral venous blood volume measurements using MRI: effects of magnetic field variation. *Magn Reson Med*. 2002;47:958-966.
26. An H, Lin W. Impact of intravascular signal on quantitative measures of cerebral oxygen extraction and blood volume under normo- and hypercapnic conditions using an asymmetric spin echo approach. *Magn Reson Med*. 2003;50:708-716.
27. Sohlin M, Schad LR. Theoretical prediction of parameter stability in quantitative BOLD MRI: dependence on SNR and sequence parameters. Paper Presented at: Proceedings of 18th Annual Meeting of ISMRM 2009.
28. Christen T, Schmiedeskamp H, Straka M, Bammer R, Zaharchuk G. Measuring brain oxygenation in humans using a multiparametric quantitative blood oxygenation level dependent MRI approach. *Magn Reson Med*. 2012;68:905-911.
29. Kaczmarz S, Hyder F, Preibisch C. Oxygen extraction fraction mapping with multi-parametric quantitative BOLD MRI: reduced transverse relaxation bias using 3D-GraSE imaging. *Neuroimage*. 2020;220:9.
30. Kaczmarz S, Goettler J, Zimmer C, Hyder F, Preibisch C. Characterizing white matter fiber orientation effects on multi-parametric quantitative BOLD assessment of oxygen extraction fraction. *J Cereb Blood Flow Metab*. 2020;40:760-774.
31. Blockley NP, Stone AJ. Improving the specificity of R2' to the deoxyhaemoglobin content of brain tissue: prospective correction of macroscopic magnetic field gradients. *Neuroimage*. 2016;135:253-260.
32. Preibisch C, Volz S, Anti S, Deichmann R. Exponential excitation pulses for improved water content mapping in the presence of background gradients. *Magn Reson Med*. 2008;60:908-916.
33. Yablonskiy DA, Sukstanskii AL, Luo J, Wang X. Voxel spread function method for correction of magnetic field inhomogeneity effects in quantitative gradient-echo-based MRI. *Magn Reson Med*. 2013;70:1283-1292.
34. Ulrich X, Yablonskiy DA. Separation of cellular and BOLD contributions to T2* signal relaxation. *Magn Reson Med*. 2016;75:606-615.
35. Stone AJ, Holland NC, Berman AJ, Blockley NP. Simulations of the effect of diffusion on asymmetric spin echo based quantitative BOLD: An investigation of the origin of deoxygenated blood volume overestimation. *Neuroimage*. 2019;201:116035.
36. Kiselev V, Posse S. Analytical model of susceptibility-induced MR signal dephasing: effect of diffusion in a microvascular network. *Magn Reson Med*. 1999;41:499-509.
37. Dickson JD, Ash TWJ, Williams GB, et al. Quantitative BOLD: the effect of diffusion. *J Magn Reson Imaging*. 2010;32:953-961.
38. Tricco AC, Lillie E, Zarin W, et al. PRISMA extension for scoping reviews (PRISMA-ScR): checklist and explanation. *Ann Intern Med*. 2018;169:467-473.
39. Moher D, Liberati A, Tetzlaff J, Altman DG. PRISMA group* t. preferred reporting items for systematic reviews and meta-analyses: the PRISMA statement. *Ann Intern Med*. 2009;151:264-269.
40. Stadlbauer A, Marhold F, Oberndorfer S, et al. Radiophysiomics: brain tumors classification by machine learning and physiological MRI data. *Cancer*. 2022;14:2363.
41. Bouvier J, Detante O, Tahon F, et al. Reduced CMRO2 and cerebrovascular Reserve in Patients with Severe Intracranial Arterial Stenosis: a combined multiparametric qBOLD oxygenation and BOLD fMRI study. *Hum Brain Mapp*. 2015;36:695-706.
42. Bennani-Baiti B, Pinker K, Zimmermann M, et al. Non-invasive assessment of hypoxia and neovascularization with MRI for identification of aggressive breast cancer. *Cancer*. 2020;12:14.
43. Stadlbauer A, Mouridsen K, Doerfler A, et al. Recurrence of glioblastoma is associated with elevated microvascular transit time heterogeneity and increased hypoxia. *J Cereb Blood Flow Metab*. 2018;38:422-432.
44. Stadlbauer A, Marhold F, Oberndorfer S, et al. Metabolic tumor microenvironment characterization of contrast enhancing brain tumors using physiologic MRI. *Metabolites*. 2021;11:668.
45. Stadlbauer A, Oberndorfer S, Heinz G, et al. Hypoxia and microvascular alterations are early predictors of IDH-mutated anaplastic glioma recurrence. *Cancer*. 2021;13:17.
46. Stadlbauer A, Zimmermann M, Doerfler A, et al. Intratumoral heterogeneity of oxygen metabolism and neovascularization uncovers 2 survival-relevant subgroups of IDH1 wild-type glioblastoma. *Neuro Oncol*. 2018;20:1536-1546.
47. Stadlbauer A, Zimmermann M, Kitzwogerer M, et al. MR imaging-derived oxygen metabolism and neovascularization characterization for grading and IDH gene mutation detection of gliomas. *Radiology*. 2017;283:798-808.
48. Heynold E, Zimmermann M, Hore N, et al. Physiological MRI biomarkers in the differentiation between glioblastomas and solitary brain metastases. *Mol Imaging Biol*. 2021;23:787-795.
49. Stadlbauer A, Heinz G, Oberndorfer S, et al. Physiological MRI of microvascular architecture, neovascularization activity, and oxygen metabolism facilitate early recurrence detection in patients with IDH-mutant WHO grade 3 glioma. *Neuroradiology*. 2022;64:265-277.
50. Stadlbauer A, Kinfe TM, Eyupoglu I, et al. Tissue hypoxia and alterations in microvascular architecture predict glioblastoma recurrence in humans. *Clin Cancer Res*. 2021;27:1641-1649.
51. Bauer S, Wagner M, Seiler A, et al. Quantitative T2'-mapping in acute ischemic stroke. *Stroke*. 2014;45:3280-3286.

52. Seiler A, Lauer A, Deichmann R, et al. Complete restitution of the ischemic penumbra after successful thrombectomy a pilot study using quantitative MRI. *Clin Neuroradiol*. 2019;29:415-423.
53. Stadlbauer A, Merkel A, Zimmermann M, et al. Intraoperative magnetic resonance imaging of cerebral oxygen metabolism during resection of brain lesions. *World Neurosurg*. 2017;100:388-394.
54. Seiler A, Deichmann R, Pfeilschifter W, Singer OC, Wagner M. Oxygen-sensitive MRI in unilateral carotid high-grade occlusive disease: No relationship between signal alterations in quantitative T2' mapping and cerebral blood volume within perfusion-restricted tissue. *Eur Stroke J*. 2016;1:497.
55. Kaczmarz S, Gottler J, Petr J, et al. Hemodynamic impairments within individual watershed areas in asymptomatic carotid artery stenosis by multimodal MRI. *J Cereb Blood Flow Metab*. 2021;41:380-396.
56. Kufer J, Preibisch C, Epp S, et al. Imaging effective oxygen diffusivity in the human brain with multiparametric magnetic resonance imaging. *J Cereb Blood Flow Metab*. 2022;42:349-363.
57. Gottler J, Kaczmarz S, Kallmayer M, et al. Flow-metabolism uncoupling in patients with asymptomatic unilateral carotid artery stenosis assessed by multi-modal magnetic resonance imaging. *J Cereb Blood Flow Metab*. 2019;39:2132-2143.
58. Gersing AS, Ankenbrank M, Schwaiger BJ, et al. Mapping of cerebral metabolic rate of oxygen using dynamic susceptibility contrast and blood oxygen level dependent MR imaging in acute ischemic stroke. *Neuroradiology*. 2015;57:1253-1261.
59. Toth V, Preibisch C, Den Hollander J, Forschler A, Kooijman H, Zimmer C. MR imaging of hypoxia in brain tumors. *Interv Neuroradiol*. 2011;1:207.
60. Reitz LY, Inglese M, Fiehler J, et al. Quantitative T2' imaging in patients with clinically isolated syndrome. *Acta Neurol Scand*. 2012;126:357-363.
61. Saitta L, Heese O, Forster AF, et al. Signal intensity in T2' magnetic resonance imaging is related to brain glioma grade. *Eur Radiol*. 2011;21:1068-1076.
62. Winkler L, Inglese M, Fiehler J, et al. Quantitative T2'-imaging in patients with clinically isolated syndrome. *Mult Scler*. 2010;1:S104-S105.
63. Holst B, Siemonsen S, Finsterbusch J, et al. T2' imaging indicates decreased tissue metabolism in frontal white matter of MS patients. *Mult Scler*. 2009;15:701-707.
64. Geisler BS, Brandhoff F, Fiehler J, et al. Blood-oxygen-level-dependent MRI allows metabolic description of tissue at risk in acute stroke patients. *Stroke*. 2006;37:1778-1784.
65. Seiler A, Blockley NP, Deichmann R, et al. The relationship between blood flow impairment and oxygen depletion in acute ischemic stroke imaged with magnetic resonance imaging. *J Cereb Blood Flow Metab*. 2019;39:454-465.
66. Preibisch C, Shi K, Kluge A, et al. Characterizing hypoxia in human glioma: a simultaneous multimodal MRI and PET study. *NMR Biomed*. 2017;30:e3775.
67. Reilander A, Pilatus U, Schure J-R, et al. Impaired oxygen extraction and adaptation of intracellular energy metabolism in cerebral small vessel disease. *Cereb Circ Cogn Behav*. 2023;4:100162.
68. Wagner M, Magerkurth J, Volz S, et al. T2'- and PASL-based perfusion mapping at 3 tesla: influence of oxygen-ventilation on cerebral autoregulation. *J Magn Reson Imaging*. 2012;36:1347-1352.
69. Seiler A, Deichmann R, Pfeilschifter W, Hattingen E, Singer OC, Wagner M. T2-imaging to assess cerebral oxygen extraction fraction in carotid occlusive disease: influence of cerebral autoregulation and cerebral blood volume. *PLoS One*. 2016;11:16.
70. Cherukara MT, Stone AJ, Chappell MA, Blockley NP. Model-based Bayesian inference of brain oxygenation using quantitative BOLD. *Neuroimage*. 2019;202:116106.
71. Stone AJ, Harston GWJ, Carone D, Okell TW, Kennedy J, Blockley NP. Prospects for investigating brain oxygenation in acute stroke: experience with a non-contrast quantitative BOLD based approach. *Hum Brain Mapp*. 2019;40:2853-2866.
72. Fields ME, Mirro AE, Binkley MM, et al. Cerebral oxygen metabolic stress is increased in children with sickle cell anemia compared to anemic controls. *Am J Hematol*. 2022;97:682-690.
73. Fields ME, Guilliams KP, Ragan D, et al. Hydroxyurea reduces cerebral metabolic stress in patients with sickle cell anemia. *Blood*. 2019;133:2436-2444.
74. Bao DP, Zhou JH, Hao Y, et al. The effects of fatiguing aerobic exercise on the cerebral blood flow and oxygen extraction in the brain: a piloting neuroimaging study. *Front Neurol*. 2019;10:7.
75. Guilliams KP, Fields ME, Ragan DK, et al. Red cell exchange transfusions lower cerebral blood flow and oxygen extraction fraction in pediatric sickle cell anemia. *Blood*. 2018;131:1012-1021.
76. Sen S, An HY, Menezes P, et al. Increased cortical cerebral blood flow in asymptomatic human immunodeficiency virus-infected subjects. *J Stroke Cerebrovasc Dis*. 2016;25:1891-1895.
77. An HY, Ford AL, Chen YS, et al. Defining the ischemic penumbra using magnetic resonance oxygen metabolic index. *Stroke*. 2015;46:982-988.
78. Ford AL, Chin VW, Fellah S, et al. Lesion evolution and neurodegeneration in RVCL-S: a monogenic microvasculopathy. *Neurology*. 2020;95:e1918-e1931.
79. An HY, Sen S, Chen YS, Powers WJ, Lin WL. Noninvasive measurements of cerebral blood flow, oxygen extraction fraction, and oxygen metabolic index in human with inhalation of air and carbogen using magnetic resonance imaging. *Transl Stroke Res*. 2012;3:246-254.
80. Sen S, An H, Sollman M, et al. Reduction in cerebral oxygen metabolism in subcortical regions may be a biomarker of cognitive decline in people living with human immunodeficiency virus. *Eur J Neurol*. 2022;29:1062-1074.
81. Zheng J, Hasting MK, Zhang XD, et al. A pilot study of regional perfusion and oxygenation in calf muscles of individuals with diabetes with a noninvasive measure. *J Vasc Surg*. 2014;59:419-426.
82. Zheng J, Li R, Zayed MA, Yan Y, An HY, Hastings MK. Pilot study of contrast-free MRI reveals significantly impaired calf skeletal muscle perfusion in diabetes with incompressible peripheral arteries. *Vasc Med*. 2021;26:367-373.
83. Zheng J, Sorensen C, Li R, et al. Deteriorated regional calf microcirculation measured by contrast-free MRI in patients with diabetes mellitus and relation with physical activity. *Diab Vasc Dis Res*. 2021;18:14791641211029002.
84. Wang CY, Zhang R, Zhang XD, et al. Noninvasive measurement of lower extremity muscle oxygen extraction fraction

under cuff compression paradigm. *J Magn Reson Imaging*. 2016;43:1148-1158.
85. Yin YY, Zhang YY, Gao JH. Dynamic measurement of oxygen extraction fraction using a multiecho asymmetric spin echo (MASE) pulse sequence. *Magn Reson Med*. 2018;80:1118-1124.
86. Lee H, Englund EK, Wehrli FW. Interleaved quantitative BOLD: combining extravascular R2' – and intravascular R-2-measurements for estimation of deoxygenated blood volume and hemoglobin oxygen saturation. *Neuroimage*. 2018;174:420-431.
87. Waddle SL, Garza M, Ying CW, et al. Vascular space occupancy asymmetric spin echo (VASO-ASE) for non-invasive quantification of cerebral oxygen extraction fraction. *Magn Reson Med*. 2023;90:211-221.
88. Lu L, Eldeniz C, An HY, et al. Quantification of myocardial oxygen extraction fraction: a proof-of-concept study. *Magn Reson Med*. 2021;85:3318-3325.
89. Domsch S, Murle B, Weingartner S, Zapp J, Wenz F, Schad LR. Oxygen extraction fraction mapping at 3 tesla using an artificial neural network: a feasibility study. *Magn Reson Med*. 2018;79:890-899.
90. Domsch S, Mie MB, Wenz F, Schad LR. Non-invasive multiparametric qBOLD approach for robust mapping of the oxygen extraction fraction. *Z Med Phys*. 2014;24:231-242.
91. Xie S, Xiao J, Duan H, Fu L, Mo D, Zhang X. Quantitative measurement of oxygen extraction fraction by MRI in patients with cerebrovascular disease: pre- and post-surgery. *Turk Neurosurg*. 2015;25:21-28.
92. Yu L, Xie S, Xiao JX, Wang ZX, Zhang XD. Quantitative measurement of cerebral oxygen extraction fraction using MRI in patients with MELAS. *PLoS One*. 2013;8:7.
93. Wang ZX, Xiao JX, Xie S, et al. MR evaluation of cerebral oxygen metabolism and blood flow in stroke-like episodes of MELAS. *J Neurol Sci*. 2012;323:173-177.
94. An HY, Lin WL, Celik A, Lee YZ. Quantitative measurements of cerebral metabolic rate of oxygen utilization using MRI: a volunteer study. *NMR Biomed*. 2001;14:441-447.
95. Cho J, Kee Y, Spincemaille P, et al. Cerebral metabolic rate of oxygen (CMRO2) mapping by combining quantitative susceptibility mapping (QSM) and quantitative blood oxygenation level-dependent imaging (qBOLD). *Magn Reson Med*. 2018;80:1595-1604.
96. Zhao Y, Wen J, Cross AH, Yablonskiy DA. On the relationship between cellular and hemodynamic properties of the human brain cortex throughout adult lifespan. *Neuroimage*. 2016;133:417-429.
97. Cho J, Zhang J, Spincemaille P, et al. QQ-NET – using deep learning to solve quantitative susceptibility mapping and quantitative blood oxygen level dependent magnitude (QSM+qBOLD or QQ) based oxygen extraction fraction (OEF) mapping. *Magn Reson Med*. 2022;87:1583-1594.
98. Wu D, Zhou Y, Cho J, et al. The spatiotemporal evolution of MRI-derived oxygen extraction fraction and perfusion in ischemic stroke. *Front Neurosci*. 2021;15:716031.
99. Cho J, Ma YH, Spincemaille P, Pike GB, Wang Y. Cerebral oxygen extraction fraction: comparison of dual-gas challenge calibrated BOLD with CBF and challenge-free gradient echo QSM plus qBOLD. *Magn Reson Med*. 2021;85:953-961.
100. Cho J, Nguyen TD, Huang W, et al. Brain oxygen extraction fraction mapping in patients with multiple sclerosis. *J Cereb Blood Flow Metab*. 2021;42:338-348.
101. Cho J, Spincemaille P, Nguyen TD, Gupta A, Wang Y. Temporal clustering, tissue composition, and total variation for mapping oxygen extraction fraction using QSM and quantitative BOLD. *Magn Reson Med*. 2021;86:2635-2646.
102. Cho J, Zhang S, Kee Y, et al. Cluster analysis of time evolution (CAT) for quantitative susceptibility mapping (QSM) and quantitative blood oxygen level-dependent magnitude (qBOLD)-based oxygen extraction fraction (OEF) and cerebral metabolic rate of oxygen (CMRO2) mapping. *Magn Reson Med*. 2020;83:844-857.
103. Cho JH, Lee J, An HY, Goyal MS, Su Y, Wang Y. Cerebral oxygen extraction fraction (OEF): comparison of challenge-free gradient echo QSM plus qBOLD (QQ) with O-15 PET in healthy adults. *J Cereb Blood Flow Metab*. 2021;41:1658-1668.
104. Hubertus S, Thomas S, Cho J, Zhang S, Wang Y, Schad LR. Using an artificial neural network for fast mapping of the oxygen extraction fraction with combined QSM and quantitative BOLD. *Magn Reson Med*. 2019;82:2199-2211.
105. Hubertus S, Thomas S, Cho JH, Zhang S, Wang Y, Schad LR. Comparison of gradient echo and gradient echo sampling of spin echo sequence for the quantification of the oxygen extraction fraction from a combined quantitative susceptibility mapping and quantitative BOLD (QSM plus qBOLD) approach. *Magn Reson Med*. 2019;82:1491-1503.
106. Zhang QH, Sui CF, Cho JH, et al. Assessing cerebral oxygen metabolism changes in patients with preeclampsia using voxel-based morphometry of oxygen extraction fraction maps in magnetic resonance imaging. *Korean J Radiol*. 2023;24:324-337.
107. Zhuang HW, Cho JH, Chiang GCY, et al. Cerebral oxygen extraction fraction declines with ventricular enlargement in patients with normal pressure hydrocephalus. *Clin Imaging*. 2023;97:22-27.
108. Yang L, Cho J, Chen T, et al. Oxygen extraction fraction (OEF) assesses cerebral oxygen metabolism of deep gray matter in patients with pre-eclampsia. *Eur Radiol*. 2022;32:6058-6069.
109. Wengler K, Wang JH, Sosa MS, et al. Mapping hepatic blood oxygenation by quantitative BOLD (qBOLD) MRI. *Magn Reson Med*. 2019;81:3272-3282.
110. Zhang S, Cho JH, Nguyen TD, et al. Initial experience of challenge-free MRI-based oxygen extraction fraction mapping of ischemic stroke at various stages: comparison with perfusion and diffusion mapping. *Front Neurosci*. 2020;14:11.
111. Baazaoui H, Hubertus S, Maros ME, et al. Artificial neural network-derived cerebral metabolic rate of oxygen for differentiating glioblastoma and brain metastasis in MRI: a feasibility study. *Appl Sci*. 2021;11:13.
112. Chiang GC, Cho J, Dyke J, et al. Brain oxygen extraction and neural tissue susceptibility are associated with cognitive impairment in older individuals. *J Neuroimaging*. 2022;32:697-709.
113. Fujita N, Shinohara M, Tanaka H, Yutani K, Nakamura H, Murase K. Quantitative mapping of cerebral deoxyhemoglobin content using MR imaging. *Neuroimage*. 2003;20:2071-2083.
114. Oughourlian TC, Yao JW, Hagiwara A, et al. Relative oxygen extraction fraction (rOEF) MR imaging reveals higher hypoxia

in human epidermal growth factor receptor (EGFR) amplified compared with non-amplified gliomas. *Neuroradiology*. 2021;63:857-868.
115. Ellingson BM, Woodworth DC, Leu K, Salamon N, Holly LT. Spinal cord perfusion MR imaging implicates both ischemia and hypoxia in the pathogenesis of cervical spondylosis. *World Neurosurg*. 2019;128:E773-E781.
116. Lee JM, Vo KD, An HY, et al. Magnetic resonance cerebral metabolic rate of oxygen utilization in hyperacute stroke patients. *Ann Neurol*. 2003;53:227-232.
117. Eker OF,Ameli R, Makris N, et al. MRI assessment of oxygen metabolism and hemodynamic status in symptomatic intracranial atherosclerotic stenosis: a pilot study. *J Neuroimaging*. 2019;29:467-475.
118. Seiler A, Deichmann R, Noth U, et al. Oxygenation-sensitive magnetic resonance imaging in acute ischemic stroke using T2'/R2' mapping influence of relative cerebral blood volume. *Stroke*. 2017;48:1671.
119. Qiu J, Wu K, Zhu M, et al. Using quantitative MRI to study the association of isocitrate dehydrogenase (IDH) status with oxygen metabolism and cellular structure changes in glioma. *Eur J Radiol*. 2022;155:8.
120. Lee H, Wehrli FW. Whole-brain 3D mapping of oxygen metabolism using constrained quantitative BOLD. *Neuroimage*. 2022;250:118952.
121. Blockley NP, Griffeth VE, Germuska MA, Bulte DP, Buxton RB. An analysis of the use of hyperoxia for measuring venous cerebral blood volume: comparison of the existing method with a new analysis approach. *Neuroimage*. 2013;72:33-40.
122. Stone AJ, Blockley NP. Improving qBOLD based measures of brain oxygenation using hyperoxia BOLD derived measures of blood volume. *Paper Presented at: Proceedings of the 25th Annual Meeting of ISMRM*; ISMRM; 2017.
123. Craig M, Irving B, Chappell M, Croal P, Zhao M. Quantiphyse tool Images © 2017-2019 University of Oxford. Published 2019. Accessed.
124. Wang Y, Fellah S, Fields ME, et al. Cerebral oxygen metabolic stress, microstructural injury, and infarction in adults with sickle cell disease. *Neurology*. 2021;97:e902-e912.
125. An H, Ford AL, Eldeniz C, et al. Magnetic resonance oxygen metabolic index distinguishes infarct from peri-infarct tissue better than ADC and PWI in hyperacute ischemic stroke patients. *Stroke Conference*. 2012;43.
126. Hirsch NM, Toth V, Forschler A, Kooijman H, Zimmer C, Preibisch C. Technical considerations on the validity of blood oxygenation level-dependent-based MR assessment of vascular deoxygenation. *NMR Biomed*. 2014;27:853-862.
127. Goettler J, Kaczmarz S, Zimmer C, Sorg C, Preibisch C, Hyder F. Uncoupling of cerebral blood flow and oxidative metabolism in patients with asymptomatic high-grade carotid artery stenosis assessed by multi-modal MRI. *J Cereb Blood Flow Metab*. 2019;39:49-50.
128. Toth V, Forschler A, Hirsch NM, et al. MR-based hypoxia measures in human glioma. *J Neurooncol*. 2013;115:197-207.
129. Jenkinson M, Beckmann CF, Behrens TE, Woolrich MW, Smith SM. Fsl. *Neuroimage*. 2012;62:782-790.
130. Penny W, Ashburner J, Kiebel S, et al. Statistical parametric mapping: An annotated bibliography. *Wellcome Department of Cognitive Neurology*. University College London; 2001.
131. Zheng J, An H, Coggan AR, et al. Noncontrast skeletal muscle oximetry. *Magn Reson Med*. 2014;71:318-325.
132. Guilliams K, Fieldssup ME, Ragan D, et al. Anemic hypoxia causes ischemic vulnerability in the watershed of children with sickle cell disease. *Ann Neurol*. 2018;84:S264-S265.
133. Ni W, Christen T, Zun Z, Zaharchuk G. Comparison of R2′ measurement methods in the normal brain at 3 tesla. *Magn Reson Med*. 2015;73:1228-1236.
134. Wharton S, Bowtell R. Fiber orientation-dependent white matter contrast in gradient echo MRI. *Proc Natl Acad Sci*. 2012;109:18559-18564.
135. Sati P, van Gelderen P, Silva AC, et al. Micro-compartment specific T2* relaxation in the brain. *Neuroimage*. 2013;77:268-278.
136. Bulte D, Chiarelli P, Wise R, Jezzard P. Measurement of cerebral blood volume in humans using hyperoxic MRI contrast. *J Magn Reson Imaging*. 2007;26:894-899.
137. Wu L, Wu W, Tali ET, Yuh WT. Oligemia, penumbra, infarction: understanding hypoperfusion with neuroimaging. *Neuroimaging Clin*. 2018;28:599-609.
138. Guadagno JV, Donnan GA, Markus R, Gillard JH, Baron J-C. Imaging the ischaemic penumbra. *Curr Opin Neurol*. 2004;17:61-67.
139. Jiang D, Lin Z, Liu P, et al. Normal variations in brain oxygen extraction fraction are partly attributed to differences in end-tidal CO_2. *J Cereb Blood Flow Metab*. 2020;40:1492-1500.

How to cite this article: Alzaidi AA, Panek R, Blockley NP. Quantitative BOLD (qBOLD) imaging of oxygen metabolism and blood oxygenation in the human body: A scoping review. *Magn Reson Med*. 2024;1-16. doi: 10.1002/mrm.30165

APPENDIX A. DATABASE SEARCH STRATEGY (EMBASE)

1	(oxygen adj3 (extraction or saturation or metabolism)).ti,ab.
2	(qbold or quantitative bold).ti,ab.
3	MR_OEF.ti,ab.
4	(mri or "mr imaging" or "magnetic resonance" or "mr measurement*").ti,ab.
5	1 and 4
6	2 or 3
7	5 or 6
8	Limit 7 to (english language and yr = "1994-Current")